

USING AEROCAPTURE TO CO-DELIVER ORBITER AND PROBE UNDER UNCERTAINTY

Samuel W. Albert*, Hanspeter Schaub[†], and Robert D. Braun[‡]

Mission architectures combining orbiters and probes offer promising platforms for planetary science. Smallsat ride-along missions like MarCO give reason for renewed interest in co-delivery architectures. If the orbiter and probe are designed to target a single atmospheric entry trajectory, a source of navigation error and maneuver complexity for co-delivery is avoided while still enabling a shared cruise stage. Regions of feasibility are identified for this co-delivery method at Mars, subject to fundamental flight mechanics viability and a number of relevant mission constraints. The implementation of closed-loop guidance for both vehicles is demonstrated in a representative scenario. Closed-loop control authority enables mitigation of uncertainties to target a desired final state. An example mission scenario for Mars is presented that delivers four small rough landers via direct-entry and a larger orbiter via aerocapture. Various shapes and sizes may be desirable for the relative landing locations of these probes, and the impact of varying separation magnitude and timing is investigated. Finally, a Monte Carlo analysis quantifies the effect of relevant uncertainties on the relative landing locations of the probes.

INTRODUCTION

The infrequency of planetary science missions makes it desirable to maximize total science return. Missions must often trade between global remote-sensing observations from an orbiter and local *in-situ* measurements obtained by a probe. Furthermore, the design of interplanetary probes sometimes requires the support of an orbiter to relay data to Earth. Therefore, co-delivery of a probe and orbiter to interplanetary destinations is a desirable architecture, and has been successfully implemented on missions including Galileo and Cassini-Huygens. However, this approach has its own drawbacks. To set up separate arrival trajectories, either the probe experiences a long passive coast phase, the probe requires a propulsion subsystem, or the orbiter performs a divert maneuver shortly before orbit insertion. This drives an increase in risk and complexity. A novel approach is presented that uses aerocapture for orbit insertion, then designs the probe and orbiter to use the same entry state.

Aerocapture is the technique of flying through a planet's atmosphere to reduce the spacecraft's energy and capture into orbit, reducing the delta-V requirement compared to propulsive orbit insertion.¹ Typically aerocapture would require a shallower atmospheric entry state than a direct-entry probe, but by tuning the vehicles' parameters they can be designed to target identical entry conditions. The vehicles then diverge during atmospheric flight to reach their respective desired final

*PhD Student, Ann and H.J. Smead Aerospace Engineering Sciences, 3775 Discovery Drive, 429 UCB – CCAR, Boulder, CO 80303.

[†]Glenn L. Murphy Chair of Engineering, Ann and H.J. Smead Aerospace Engineering Sciences, 3775 Discovery Drive, 429 UCB – CCAR, Boulder, CO 80303. AAS Fellow.

[‡]Professor Adjunct, Ann and H.J. Smead Aerospace Engineering Sciences, University of Colorado Boulder, Colorado Center for Astrodynamics Research, 3775 Discovery Drive, 429 UCB – CCAR, Boulder, CO 80303. AAS Fellow.

states, as shown in Fig. 1. By avoiding the need to set up two separate approach trajectories, this co-delivery technique reduces maneuver complexity during approach and eliminates a source of navigation error, while still gaining the benefits of a shared cruise stage between the orbiter and probe. This is similar to the “carry your own relay” approach employed by the MarCO CubeSats for the InSight Mars lander,² except the secondary CubeSats could aerocapture into orbit rather than performing a flyby, thus greatly extending their operational lifetimes.

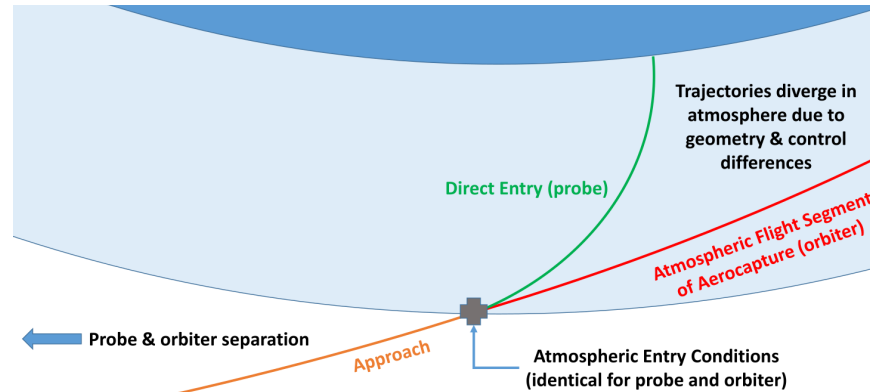


Figure 1: Diagram of the proposed co-delivery method

This paper focuses on the application of this co-delivery method to Mars planetary science missions. A broad trade study defines regions of fundamental feasibility for aerocapture and direct-entry from the same entry state at Mars for realistic ballistic coefficients and includes the values of relevant flight mechanics constraints. A single representative scenario at Mars is demonstrated for an orbiter with closed-loop bank-angle control and two versions of a probe, one with closed-loop bank-angle control and another that passively follows a ballistic trajectory. A particular mission scenario is then examined that would deliver multiple small rough landers to the Martian surface from a single aerocapture orbiter. The impact on landed geometry of varying the timing and magnitude of the separation of the probes from the orbiter is investigated, and the variation in landing locations due to representative uncertainties is quantified through a Monte Carlo analysis. The motivation for this mission design is to deliver a regional network of small science payloads to the Martian surface as a secondary ride-along with a larger mission.

DEMONSTRATING FEASIBILITY

Trade Study Results at Mars

This section broadly maps the combinations of trajectories and vehicles for which aerocapture and direct-entry from the same entry state is feasible, and computes several key constraining parameters across the trade space. This provides a starting point for further investigation of any specific mission concept, as is shown by example. This subsection summarizes results presented at the 2020 AAS Astrodynamics conference;³ full details of the methodology can be found there along with results for other planetary destinations.

A large range of trajectories are simulated for this analysis, computed by numerically integrating the three degree-of-freedom equations of motion assuming point-mass gravity, lift, and drag are the only forces acting on the vehicle^{4*}. Constant aerodynamic coefficients, constant mass, zero thrust,

*<https://github.com/salbert21/petunia>

and zero wind are assumed. The vehicle state is propagated using a variable-step Runge-Kutta numerical integration method of order 5(4).⁵ The vehicle is initialized at the atmospheric interface with an altitude of $h_{\text{atm}} = 125 \text{ km}$ and a planet-relative velocity of 6 km s^{-1} . Entry flight path angle (EFPA) and ballistic coefficient are varied as part of the trade study. EFPA is the angle between the vehicle’s planet-relative velocity vector and the local horizontal. The ballistic coefficient β is effectively a ratio of inertial to aerodynamic forces on the vehicle and is defined in Eq. 1, where m is vehicle mass, C_D is hypersonic drag coefficient, and A is reference area. Ballistic, full-lift-up, and full-lift-down trajectories are simulated at each gridpoint in this trade study. For the lifting vehicles, a lift-to-drag ratio of $L/D = 0.25$ is used to approximate the hypersonic trim L/D of the Mars Science Laboratory (MSL) and Mars 2020 entry vehicles and the known capabilities of a 70° sphere cone aeroshell.⁶

$$\beta = \frac{m}{C_D A} \quad (1)$$

Profiles of atmospheric density are taken from the nominal output of the Mars Global Reference Atmospheric Model 2010 (Mars-GRAM 2010),⁷ then linearly interpolated with altitude. To approximately characterize the effect of density variability, results include a uniform $\pm 20\%$ uncertainty in density. The actual variability in atmospheric density is not uniform with altitude, nor is it necessarily within a 20% bound; these results are included only to show a general trend of how density variability impacts the feasibility of the proposed co-delivery method. Peak heat rate, total heat load, and peak g-load are all computed for each trajectory. Heat rate is computed as convective heat flux at the stagnation point for a fully catalytic surface using the Sutton-Graves method,⁸ with a value of $1.904 \times 10^{-4} \text{ kg}^{0.5}/\text{m}$ computed for the heating coefficient.³ Apoapsis altitude is also shown for trajectories that result in an elliptical Keplerian state at atmospheric exit.

The results of this trade study are captured in Fig. 2. The black lines represent the transition between probe and orbiter trajectories, and the purple lines show the transition between orbiter and escape trajectories. The shaded regions around each line show the values for that line when the density profile is at $\pm 20\%$ of the nominal values. Thus, gridpoints to the left of the black line are probe trajectories, between the two lines are orbiter trajectories, and to the right of the purple lines are escape trajectories.

These plots allow a mission designer to tell at a glance where the proposed co-delivery method would be feasible. By definition, for the proposed co-delivery method to work a probe trajectory and an orbiter trajectory would need to both exist at the same EFPA for realistic ballistic coefficients. Thus, co-delivery scenarios are identified along vertical lines on Fig. 2 that pass through both orbiter and probe regions. Uncertainty around the delivery state can be represented as a range of possible EFPA values, and the effect of this entry corridor can also be understood from Fig. 2 by adding additional vertical lines at the minimum and maximum expected EFPA values and taking the most constrained result. Finally, the overlaid contours allow for additional constraints to be imposed. As an example, consider an EFPA of -12° with an entry corridor width of $\pm 0.25^\circ$, with a desired apoapsis altitude of at least 300 km for the orbiter and a peak heat rate limit of 50 W cm^{-2} for the probe. From Fig. 2, it can be seen that a lift-up orbiter would need a ballistic coefficient of at least 130 kg m^{-2} , and a ballistic probe would require a ballistic coefficient no greater than 100 kg m^{-2} . These values are approximate and any particular mission scenario requires significant further analysis, but this example illustrates how the results in Fig. 2 can be interpreted subject to a variety of user-defined constraints.

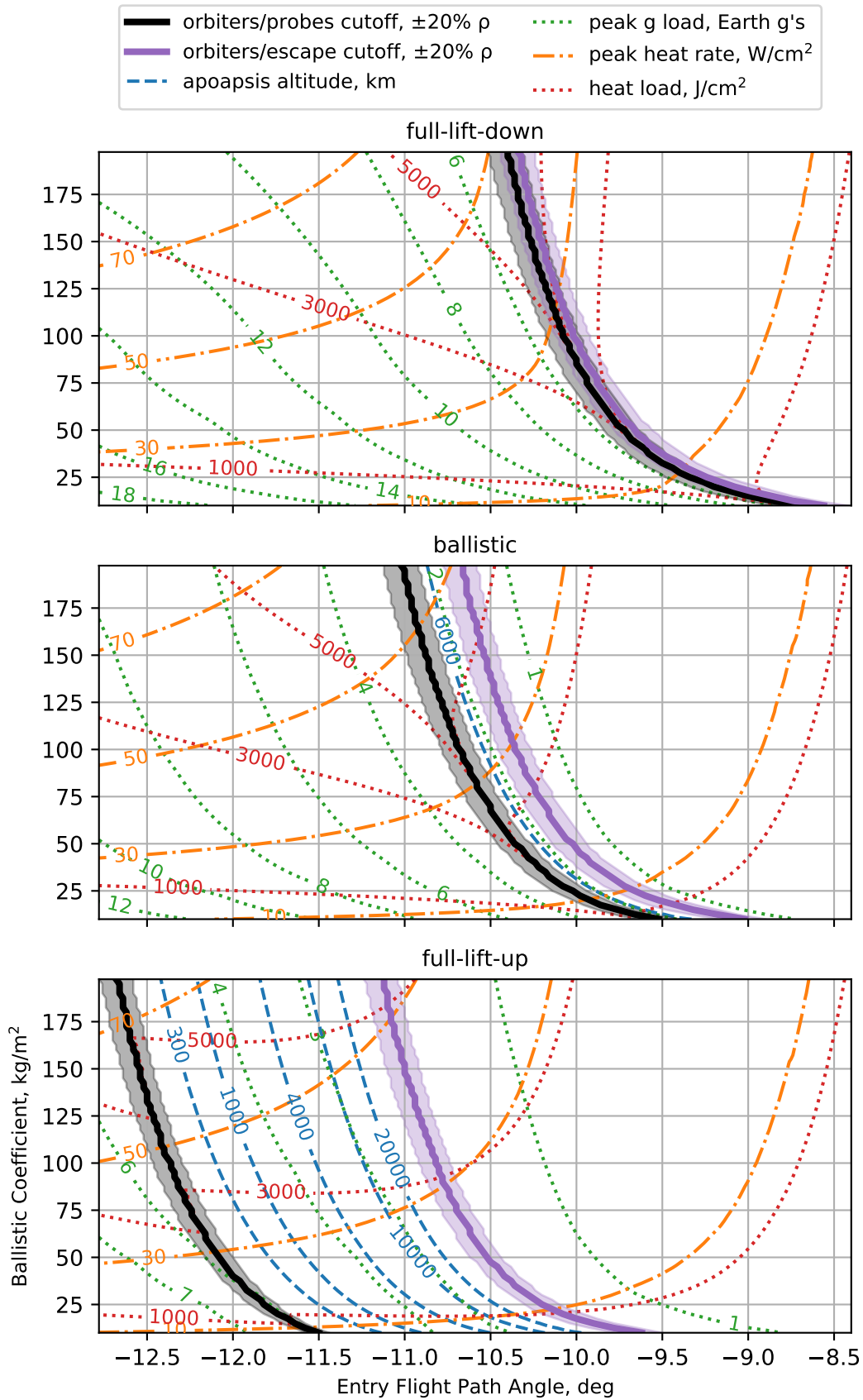


Figure 2: Feasibility space for Mars, 6 km s⁻¹ relative entry velocity

Representative Scenario With Guidance

The feasibility results shown so far only include open-loop control in the form of full-lift-up or -down trajectories. Any real aerocapture mission will require closed-loop control to target the desired final state accurately and in the presence of uncertainties. In this subsection, a nominal scenario with guidance is implemented at Mars. This subsection summarizes results presented in [9], which also includes more details on the guidance implementation and shows guidance performance under uncertainty for this scenario.

As outlined in the example above, Fig. 2 shows that a lifting vehicle with ballistic coefficient of $\beta = 130 \text{ kg m}^{-2}$ and $L/D = 0.25$ can achieve aerocapture with a low apoapsis from an EFPA of -12° . Likewise, it was shown that a ballistic probe with $\beta = 35 \text{ kg m}^{-2}$ could achieve direct-entry at the same EFPA. To target specific desired final states, both vehicles are now implemented with closed-loop guidance using bank-angle modulation for control, the same technique employed by the MSL and Mars 2020 missions.^{6, 10} A version of Mode 1 of the Fully-Numerical Predictor-corrector Aerocapture Guidance (FNPAG) scheme developed by Lu et. al is implemented for the orbiter,¹¹ and Fully-Numerical Predictor-corrector Entry Guidance (FNPEG), developed by Lu,¹² is used for the guided probe. Several simplifying assumptions are made for both vehicles, including that only longitudinal targeting is considered and the bank-angle is updated instantaneously.

Nominal trajectories computed by these guidance schemes are shown in Fig. 3. The orbiter targets a 250 km altitude circular orbit, and the guided probe targets final altitude, velocity, and range values of 15 km, 300 m s^{-1} , and 700.8 km, respectively. The switching time, where the orbiter transitions from a lift-up orientation to lift-down, is marked with the circle. A third trajectory is also included for a passive probe that has the same entry state and properties as the guided probe, except that it is ballistic ($L/D = 0$) and thus exerts no control during its atmospheric flight.

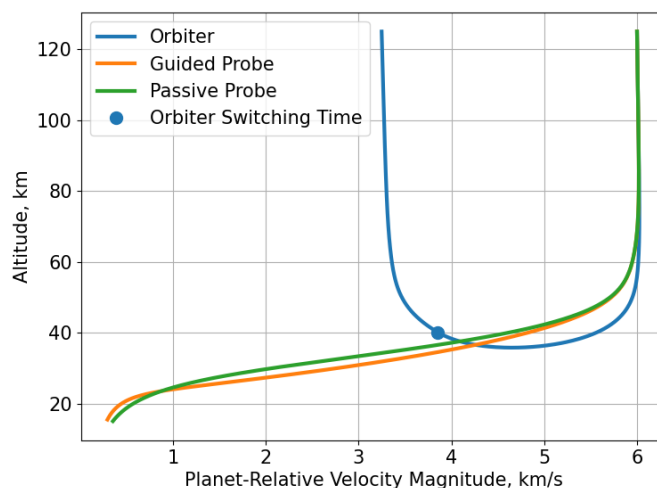


Figure 3: Nominal trajectories for the orbiter, guided lifting probe, and passive ballistic probe

This nominal scenario is included here to demonstrate that, although the trajectories represented in Fig. 2 fly bounding cases in an open-loop sense, corresponding co-delivery scenarios exist that use closed-loop guidance to target a specific final state. While the trajectories shown here are for a nominal scenario, closed-loop guidance would enable the vehicles to still target their final states

in the presence of delivery errors, atmospheric variability, and uncertainties in the vehicles' aerodynamic properties. Moreover, while the passive ballistic probe would lack any ability to mitigate these uncertainties, the resulting dispersions in its final states may be acceptable for some science missions that do not require precise landing.⁹

EXAMPLE MISSION SCENARIO: MARS MULTIPROBE MISSION

This section presents a specific mission concept that would take advantage of the proposed co-delivery method in order to collect valuable science data on the Martian surface. This mission delivers multiple small probes to the Martian surface via ballistic direct-entry trajectories and a larger orbiter via lift-modulated aerocapture. These probes form a regional network of static landers, able to make simultaneous measurements at locations on the surface separated by tens or hundreds of kilometers, and the orbiter provides a telecommunications relay back to Earth as well as a platform for additional complementary science. A variety of science investigations may be uniquely enabled by combining this architecture with instruments that fit in a small package, microseismometers and meteorological suites being two examples.^{13,14}

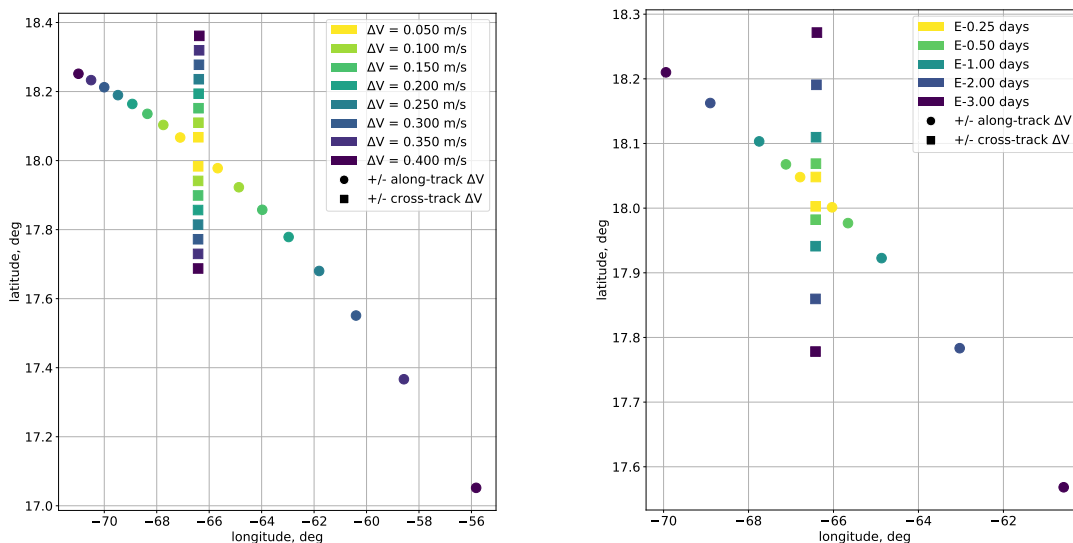
For this analysis, the orbiter is assumed to have a 70° sphere-cone aeroshell with offset center of gravity akin to MSL,⁶ with $\beta = 130 \text{ kg m}^{-2}$ and $L/D = 0.25$. The probes are based on the Small High Impact Energy Landing Device (SHIELD) concept, a ballistic vehicle with approximately $\beta = 10 \text{ kg m}^{-2}$.¹⁵ This small probe is a rough lander designed to reduce the cost and complexity of delivering 6 kg payloads to the Martian surface by forgoing parachutes and any terminal descent system in favor of a low ballistic coefficient and crushable material, resulting in landing decelerations on the order of 1000 Earth g's.¹⁵ For this mission concept, four identical probes are co-delivered with a single orbiter from a nominal due-East entry at -77.58° longitude, 18.38° latitude with EFPA of -12° and entry velocity of 6 km s^{-1} . Based on the concept of a regional seismic or meteorological network, it is assumed that the approximate relative landing locations of the probes is important, but not a precise delivery to a pre-determined site. The orbiter would enable precise positioning after landing.

Varying Separation Magnitude and Timing

If the identical probes were truly delivered to the same entry state as each other and the orbiter, they would fail to spread out on the surface and would risk collision in the atmosphere. Thus, the probes need to separate away from the orbiter and each other at some point prior to atmospheric entry such that their landing locations satisfy requirements on geometry and relative separation distances for the probe network. Furthermore, the probes should impart a near-zero net ΔV on the orbiter to avoid knocking its aerocapture trajectory off course. In this analysis, it is assumed that the probe separations are achieved by mechanical means such as springs or pyrotechnic bolts, which could in theory be balanced in pairs in opposite directions across the orbiter's center of gravity.

The timing and magnitude of the probe separation events are key mission design parameters. If the separation occurs too late, the required ΔV magnitude becomes relatively large in order to achieve separation on the surface, and there may be insufficient time to measure and correct any error introduced to the orbiter trajectory. An early separation would reduce the required ΔV magnitude and leave time for potential reorientation and navigation updates for the orbiter. However, the relatively long coast phase amplifies the effect of any off-nominal separation ΔV on the probes' trajectories and requires longer battery life prior to landing.

To gain insight into these tradeoffs, four probes are simulated with varying separation ΔV magnitudes and separation times. The probes are back-propagated from the nominal entry state until the separation time, the ΔV is applied, and then the probes are propagated until impact with the Martian surface. The direction in which the ΔV is applied is also a key design choice; in this study, separation is considered along two orthogonal vectors, along-track and cross-track. For each of those two vectors, a pair of probes separates in the positive and negative directions along that vector. The ΔV magnitude varies from 5 to 40 cm s^{-1} at a nominal separation time of E-1 day, and the separation time varies from 0.25-3 days at a nominal ΔV of 10 cm s^{-1} . The resulting landing locations are shown in Fig. 4, and for each permutation the minimum and maximum great-circle distances between any two landing locations are shown in Tables 1 and 2.



(a) Separation at E-1 day, varying ΔV

(b) $\Delta V = 0.100 \text{ m s}^{-1}$, varying separation time

Figure 4: Landing locations of the four probes

Table 1: Landing Site Distances for Probe Separation at E-1 day, Varying ΔV

ΔV , cm/s	Minimum Distance, km	Maximum Distance, km
5	5.006	80.787
10	10.011	162.831
15	15.016	247.581
20	20.021	336.941
25	25.026	433.777
30	30.031	543.062
35	35.035	675.207
40	40.039	859.503

From the results in Fig. 4, it is clear that changes in landing location are significantly more sensitive to ΔV in the along-track direction than ΔV in the cross-track direction. Note that while in this analysis along-track and cross-track correspond primarily to longitudinal and latitudinal separation, respectively, this is because of the due-East heading angle assumed for this particular scenario. A

Table 2: Landing Site Distances for $\Delta V = 0.100 \text{ m s}^{-1}$, Varying Separation Time

Separation Time, days	Minimum Distance, km	Maximum Distance, km
E-0.25	2.694	42.504
E-0.5	5.151	82.544
E-1	10.011	162.831
E-2	19.674	331.883
E-3	29.311	529.586

wide range of 2D landed geometries on the scale of tens or hundreds of kilometers could be achieved based on these results by tuning the timing and ΔV magnitude of the separation for each pair of probes, with additional geometries accessible by separating in other directions.

One notable feature of these results is the approximately linear relationship between ΔV magnitude and the resulting landing locations, as can be observed by inspection of Tables 1 and 2. Although the interplanetary and entry dynamics are nonlinear, the changes in velocity considered here are small enough compared to the 6 km s^{-1} entry velocity that these perturbations away from the nominal case result in approximately linear variations in the final state. For the range of values considered in this analysis, the above also holds true for changes in the timing of a perturbation of a given size. This phenomenon is similar to the linearization used for B-plane targeting of interplanetary trajectories, and could enable a linearized iterative approach to targeting specific landing geometries under given constraints.

Performance Under Uncertainty

Having considered a range of nominal trajectories, this subsection quantifies the effects of representative uncertainties in the separation ΔV , vehicle aerodynamics, and atmospheric density profile through a 500-trial Monte Carlo analysis. The separation time is set to E-1 day, with a nominal separation magnitude of $\Delta V = 10 \text{ cm s}^{-1}$. The ΔV magnitude is then dispersed with a uniform error of $\pm 10\%$, noting that the timing and direction of the ΔV are held as deterministic. The state immediately prior to separation is also considered deterministic, even though delivery and navigation error would generally play a role, in order to separately consider the effect of uncertainty beginning with the separation event. This is reasonable here because small errors in the state prior to separation would shift all landing locations in a similar way, with only a minor effect on the resulting landed geometry. The ballistic coefficient of the probes is dispersed with uniform error of $\pm 5\%$, and because the probes are assumed to be manufactured identically the dispersed ballistic coefficient is identical between all four probes. Finally, in each trial the density profile is randomly generated using the Monte Carlo functionality of Mars-GRAM 2010,⁷ kept at default settings for the nominal entry latitude and longitude. This study only presents Monte Carlo results for the passive probes, but the orbiter could use bank-angle modulation to accurately target its desired orbit under uncertainty for this same trajectory and vehicle.⁹

Figure 5 shows the landing locations of the four probes for each of the 500 trials. The minimum separation distance has a mean of 9.98 km and standard deviation of 0.407 km with a range of [9.06, 10.87] km. The maximum separation distance has a mean of 163 km and standard deviation of 7.30 km with a range of [147, 180] km. Thus, for both metrics an error of one standard deviation equates to a percent error of about 5%. The much smaller spread for the minimum separation compared to the maximum occurs because for this nominal geometry the two closest probes are the cross-track pair, and the landing locations are less sensitive to changes in cross-track ΔV than along-track ΔV . For a similar reason, the grouping of locations for cross-track separated probes

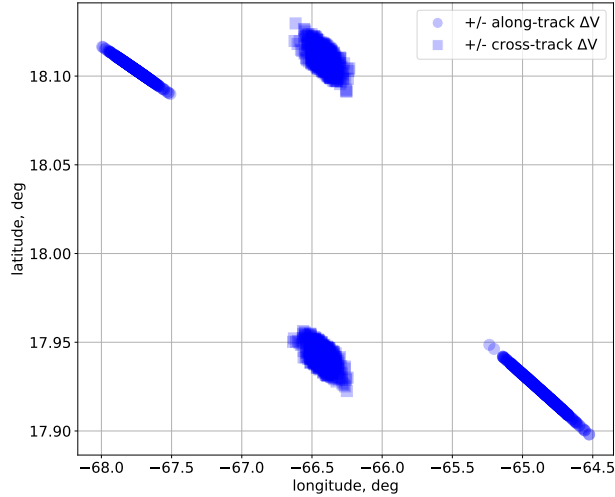


Figure 5: Landing locations of all four probes for 500-trial Monte Carlo analysis

appear more random due to the influence of uncertain ballistic coefficients and atmospheric density, whereas for the along-track cases the high sensitivity to changes in ΔV outweighs the impact of the other uncertainties and the variation follows a path similar to that seen in Fig. 4a.

These comparisons reflect an inherent tradeoff for this mission architecture: for trajectory designs that use small ΔV separations to achieve a large change in landing location, small separation ΔV errors will have a large impact. Though not considered in this study, variation in the direction of the separation ΔV would have a significant impact as well. Although rough landers like SHIELD benefit from being tolerant to a relatively large flight envelope by eliminating parachutes and accepting higher landing decelerations, they also sacrifice the ability to mitigate dispersions by opting to fly passively through the atmosphere. The acceptable ranges of entry conditions and relative landing locations depend on detailed vehicle design and the particular science case, respectively. That being said, for a science case that requires relative lander separations on the order of hundreds of kilometers but does not need precise targeting for landing locations, variation in the low tens of kilometers may be within an acceptable range.

CONCLUSION

A novel co-delivery method for orbiters and probes is presented and shown to be feasible for a wide range of trajectories at Mars, and values of peak heat rate, total heat load, peak g-load, and apoapsis altitude are computed across the trade space. A single nominal scenario is developed that incorporates closed-loop guidance for both vehicles, which enables them to accurately target their desired final states under uncertainty. One mission scenario of interest is an MSL-class vehicle that delivers multiple small rough landers via ballistic direct-entry trajectories before performing aerocapture to enter orbit. These landers could form a network on the scale of tens or hundreds of kilometers to perform surface science at a regional scale, and this geometry could be achieved using mechanical separation to impart a ΔV in the low tens of centimeters per second a day or more before entry. Although these passive probes are subject to numerous uncertainties, the effects

on relative landing locations are within about 5-15% which may be acceptable for some science missions.

ACKNOWLEDGMENTS

The first author thanks Dr. Don Banfield and Dr. Mark Panning for their input on relevant science investigations for the presented mission concept, and Dr. Chad Edwards for information on the SHIELD concept. This work was supported by a NASA Space Technology Research Fellowship.

REFERENCES

- [1] J. L. Hall, A. N. Noca, and R. W. Bailey, “Cost-Benefit Analysis of the Aerocapture Mission Set,” *Journal of Spacecraft and Rockets*, Vol. 42, No. 2, 2005, pp. 309–320.
- [2] S. W. Asmar and S. Matousek, *Mars Cube One (MarCO): Shifting the Paradigm in Relay Deep Space Operation*, ch. OCFE - Mission Ops Concept I, pp. 1–7. American Institute of Aeronautics and Astronautics, 2016.
- [3] S. W. Albert, R. D. Braun, and H. Schaub, “AeroDrop: Prospects and Challenges for Co-Delivery of Probe and Orbiter via Aerocapture,” *AAS/AIAA Astrodynamics Specialist Conference, Lake Tahoe, CA*, 2020, pp. 1–19.
- [4] N. X. Vinh, A. Busemann, and R. D. Culp, *Hypersonic and Planetary Entry Flight Mechanics*, ch. 2, pp. 26–27. The University of Michigan Press, 1980.
- [5] J. Dormand and P. Prince, “A family of embedded Runge-Kutta formulae,” *Journal of Computational and Applied Mathematics*, Vol. 6, No. 1, 1980, pp. 19–26, [https://doi.org/10.1016/0771-050X\(80\)90013-3](https://doi.org/10.1016/0771-050X(80)90013-3).
- [6] D. Way, R. Powell, A. Chen, A. Steltzner, M. San Martin, P. Burkhart, and G. Mendeck, “Mars Science Laboratory: Entry, Descent, and Landing System Performance,” *IEEE Aerospace Conference Proceedings*, March 2006, pp. 1–19.
- [7] H. Justh, “Mars Global Reference Atmospheric Model 2010 Version: Users Guide,” Tech. Rep. NASA/TM—2014–217499, NASA, 2014.
- [8] K. Sutton and R. A. Graves, “A General Stagnation-Point Convective-Heating Equation for Arbitrary Gas Mixtures,” Tech. Rep. TR R-376, NASA, 1971.
- [9] S. W. Albert, R. D. Braun, and H. Schaub, “Flight Mechanics Feasibility Assessment for Co-Delivery of Direct-Entry Probe and Aerocapture Orbiter,” *Submitted to Journal of Spacecraft and Rockets*, 2021.
- [10] P. Brugarolas, “Guidance, Navigation and Control for the Entry, Descent, and Landing of the Mars 2020 Mission,” *40th Annual AAS Guidance and Control Conference, Breckenridge, Colorado*, February 2017, pp. 1–12.
- [11] P. Lu, C. J. Cerimele, M. A. Tigges, and D. A. Matz, “Optimal Aerocapture Guidance,” *Journal of Guidance, Control, and Dynamics*, Vol. 38, No. 4, 2015, pp. 553–565, 10.2514/1.G000713.
- [12] P. Lu, “Entry Guidance: A Unified Method,” *Journal of Guidance, Control, and Dynamics*, Vol. 37, No. 3, 2014, pp. 713–728, 10.2514/1.62605.
- [13] C. Nunn, W. T. Pike, I. M. Standley, S. B. Calcutt, S. Kedar, and M. P. Panning, “Standing on Apollo’s Shoulders: a Microseismometer for the Moon,” *The Planetary Science Journal*, Vol. 2, No. 1, 2021, p. 36.
- [14] S. Rafkin, “The Atmospheric Characterization for Exploration and Science (ACES) instrument suite for Mars,” *2015 IEEE Aerospace Conference*, 2015, pp. 1–6, 10.1109/AERO.2015.7119061.
- [15] N. Barba, T. Komarek, R. Woolley, L. Giersch, V. Stamenković, M. Gallagher, and C. D. Edwards, “Mars Small Spacecraft Studies: Overview,” *2019 IEEE Aerospace Conference*, 2019, pp. 1–10, 10.1109/AERO.2019.8741735.